ELSEVIER

Journal of Power Sources 111 (2002) 320–328

JOURNAL OF POWER SOURCES

www.elsevier.com/locate/jpowsour

An electrolyte model for ceramic oxygen generator and solid oxide fuel cell

S.H. Chan*, X.J. Chen, K.A. Khor

Fuel Cell Strategic Research Programme, School of Mechanical and Production Engineering, Nanyang Technological University of Singapore, 50 Nanyang Avenue, Singapore 639798, Singapore

Received 13 March 2002; accepted 1 June 2002

Abstract

A mathematical model describing the distribution of the concentrations of electrons and electron holes and the potential along the thickness of electrolyte is developed. This model facilitates the study of various electrolyte materials and the effects of operating temperature, oxygen partial pressure and electrolyte thickness on oxygen semi-permeability. The model is applied to a study of the performance of a ceramic oxygen generators (CoGs) and a solid oxide fuel cells (SoFCs). In a CoG, $CO + CO_2$|electroloyte|pure O_2 and $N_2 + O_2$|electroloyte|pure O_2 are considered for a system which requires low O_2 and high O_2 semi-permeability, respectively. In a SoFC, for doped-ZrO_2 at 800 °C, the thinner the electrolyte, the higher the energy efficiency and the output power density will be at intermediate current density due to the higher Ohmic loss of the electrolyte. Thus, obtaining low O_2 semi-permeability for a thin electrolyte is also desirable in SoFC development.

Keywords: Electrolyte model; Ion-conducting membrane; Oxygen semi-permeability; Ceramic oxygen generator; Solid oxide fuel cell

1. Introduction

Doped-ZrO_2, doped-CeO_2 and doped-Bi_2O_3 are ionic conductors that have been widely considered as ideal electrolyte materials for ceramic oxygen generators and solid oxide fuel cells (SoFCs) [1–4]. Such application mainly considers the ionic behaviour of the electrolyte materials. Though they are ionic solids, the diffusion of electronic components (electrons and electron holes) across the electrolyte cannot be neglected. The diffusivity of the charge carriers depends largely on the mobility and the operating temperature. Generally, the electronic conductivity is considered to arise from the following reactions [5].

At low oxygen pressures:

$$O_O^x = \tfrac{1}{2}O_2 + V_{\ddot{O}} + 2e^- \quad (1)$$

At medium and high oxygen pressures:

$$\tfrac{1}{2}O_2 + V_{\ddot{O}} = O_O^x + 2\dot{h} \quad (2)$$

In a H_2–O_2 fuel cell environment:

$$H_2 + O_O^x = V_{\ddot{O}} + H_2O + 2e^- \quad (3)$$

Under normal CoG and SoFC operating conditions, the concentrations of oxygen ions and oxygen vacancies remain almost constant [6]. Thus, based upon Eqs. (1) and (2), the concentrations of free electrons and electron holes at the gas|electrolyte interface can be written as:

$$c_{e^-} = k_{e^-} p_{O_2}^{-1/4} \quad (4)$$

$$c_{\dot{h}} = k_{\dot{h}} p_{O_2}^{1/4} \quad (5)$$

where the reaction rate constants k_{e^-} and $k_{\dot{h}}$ are temperature-dependent parameters.

Since there is mixed ionic and electronic conducting behaviour in these oxide electrolytes, the electronic current can flow through the electrolyte even at the open-circuit condition. Thus, the terminal voltage is somewhat lower than the theoretical voltage of the cell reaction and the performance of the cell decreases with the increase of electronic conductivity [7].

Though electronic conductivity of solid oxides is undesirable for the electrolyte used in SoFCs, such mixed-conductive behaviour has been extensively researched for gas-separation membranes, which can work without the need of electrodes and externally applied current [8–10]. In this case, applying a differential oxygen pressure across the electrolyte can establish concentration gradients of free electron and electron holes across the electrolyte. Thus, free electrons or electron holes diffuse through the ceramic membrane naturally, and the oxide ions, which migrate in the counter direction, will compensate the electrical charge. The net effect is a flux of oxygen through the membrane,

* Corresponding author. Tel.: +65-790-4862; fax: +65-791-1859.
E-mail address: mshchan@ntu.edu.sg (S.H. Chan).

0378-7753/02/$ – see front matter
PII: S0378-7753(02)00318-X

Nomenclature

c_{e^-}	concentration of free electron (mol cm^{-3})
$c_{\dot{h}}$	concentration of electron–hole (mol cm^{-3})
$\tilde{C}_{e^-}$	dimensionless concentration of free electron
$\tilde{C}_{\dot{h}}$	dimensionless concentration of electron–hole
D_i	diffusion rate of species i (cm^2 s^{-1})
E_{e^-}	activation energy of free electron (eV)
$E_{\dot{h}}$	activation energy of electron–hole (eV)
F	Faradic constant, 96 486 C mol^{-1}
ΔH_{V_O}	activation energy of oxygen vacancy (eV)
I	current density (A cm^{-2})
J	mass flux (mol cm^{-2} s^{-1})
k_{e^-}	free-electron reaction rate constant
$k_{\dot{h}}$	electron hole reaction rate constant
k	Boltzman constant, 1.38×10^{-23} J K^{-1}
L	electrolyte thickness (cm)
p	oxygen partial pressure (atm)
R_A	area polarisation resistance of anode (Ω cm^2)
R_C	area polarisation resistance of cathode (Ω cm^2)
R_e	area electronic resistance (Ω cm^2)
R_i	area ionic resistance (Ω cm^2) or homogeneous reaction rate (mol cm^{-3} s^{-1})
T	temperature (K)
u_i	mobility of species i
V	gas volume (cm^3)
z	electron number

Greek symbols

ϕ	inner potential of the electrolyte (V)
σ	electrical conductivity (S cm^{-1})
υ	gas flow velocity (cm s^{-1})

Subscripts

A	anode
C	cathode
e^-	free electron
$\dot{h}$	electron–hole
$V_{\ddot{O}}$	oxygen vacancy

which is the so-called 'oxygen electrochemical semi-permeability'.

In this study, an electrolyte conduction model which considers the electronic conductivity is developed to investigate the transport phenomena of free electrons and electron holes through the electrolyte, and to evaluate systemically the effect of electronic conduction on the performance of CoGs and SoFCs.

2. Electrolyte model considering the electronic conductivity

With reference to the schematic diagram shown in Fig. 1, a one-dimensional electrolyte model was developed based on the following assumptions:

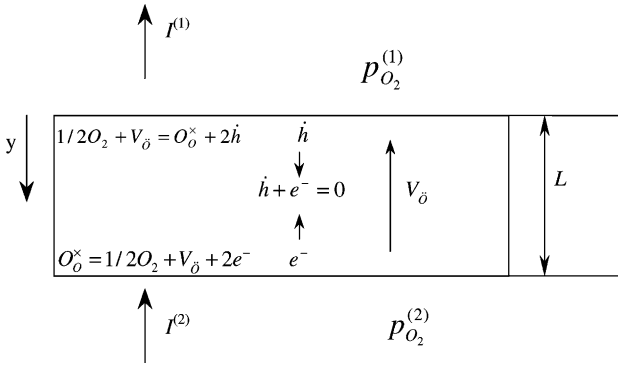

Fig. 1. Schematic diagram of electrolyte reactions with transport of charge species.

(i) the concentration of oxygen vacancies in the electrolyte is constant and is independent of the oxygen partial pressure in the range of 10^{-18} to 10 atm;
(ii) the temperature is uniform throughout the electrolyte;
(iii) the ionic and electronic conductivities are uniform throughout the electrolyte, and are temperature-dependent parameters;
(iv) the current and species concentrations (electrons and electron holes) vary only along the y-axis;
(v) the mobility of the charge species is uniform throughout the electrolyte;
(vi) oxygen surface exchange imposes no constraints on the ionic transport.

The Nernst–Planck equation is used to describe the flux of species, i.e.

$$J_i = -z_i u_i F c_i \nabla\phi - D_i \nabla c_i \tag{6}$$

which states that a dissolved species can move by migration and diffusion. The current density, I arising from the motion of the charged particles is given by:

$$I = F\sum_i z_i J_i \tag{7}$$

All charge species within the electrolyte must obey the conservation of mass, i.e.

$$\nabla J_i + R_i = 0 \tag{8}$$

Combining Eqs. (4) and (5) can eliminate the dependency on oxygen pressure, thus

$$c_{e^-} \times c_{\dot{h}} = k_{e^-} p_{O_2}^{-1/4} \times k_{\dot{h}} p_{O_2}^{1/4} = k_{e^-} k_{\dot{h}} = K(T) \tag{9}$$

The dimensionless concentrations of free electrons and electron holes are defined as:

$$\tilde{C}_{e^-} \frac{c_{e^-}}{c_{e^-}^{(2)}} \quad \text{and} \quad \tilde{C}_{\dot{h}} \frac{c_{\dot{h}}}{c_{\dot{h}}^{(1)}} \tag{10}$$

The requirement of electroneutrality of the electrolyte yields:

$$\sum_i z_i c_i = 0 \tag{11}$$

Since the concentration of oxygen vacancies is constant ($\nabla c_{V_{\ddot{O}}} = 0$ and $R_{V_{\ddot{O}}} = 0$), combining Eqs. (6) and (8) gives Eq. (12). Assuming homogenous reaction between the free electrons and electron holes within the electrolyte ($R_{e^-} = R_{\dot{h}}$) and using Nernst–Einstein relation $D_i = u_i R_u T$ and combining Eqs. (6), (8) and (10) written for respective free electrons and electron holes yields Eq. (13). Finally, combining Eqs. (9) and (10) yields Eq. (14):

$$\nabla^2 \phi = 0 \tag{12}$$

$$\frac{\sigma_{\dot{h}}^{(1)}}{z_{\dot{h}} F} \nabla \tilde{C}_{\dot{h}} \nabla \phi - \frac{\sigma_{e^-}^{(2)}}{z_{e^-} F} \nabla \tilde{C}_{e^-} \nabla \phi - \frac{R_u T \sigma_{\dot{h}}^{(1)}}{z_{\dot{h}}^2 F^2} \nabla^2 \tilde{C}_{\dot{h}} - \frac{R_u T \sigma_{e^-}^{(2)}}{z_{e^-}^2 F^2} \nabla^2 \tilde{C}_{e^-} = 0 \tag{13}$$

$$\tilde{C}_{\dot{h}} \tilde{C}_{e^-} = \left(\frac{p_{O_2}^{(2)}}{p_{O_2}^{(1)}} \right)^{1/4} \tag{14}$$

To solve for ϕ, $\tilde{C}_{e^-}$ and $\tilde{C}_{\dot{h}}$ and the following six boundary conditions are required:

$$\phi^{(2)} = 0 \tag{15a}$$

$$\tilde{C}_{\dot{h}}^{(2)} = \left(\frac{p_{O_2}^{(2)}}{p_{O_2}^{(1)}} \right)^{1/4} \tag{15b}$$

$$\tilde{C}_{e^-}^{(2)} = 1 \tag{15c}$$

$$I^{(1)} = -I^{(2)} = -(\sigma_{e^-}^{(2)} \tilde{C}_{e^-} + \sigma_{\dot{h}}^{(1)} \tilde{C}_{\dot{h}} + \sigma_{V_O}) \nabla \phi^{(1)} - \frac{R_u T}{F} \left(\frac{\sigma_{e^-}^{(2)}}{z_{e^-}} \nabla \tilde{C}_{e^-}^{(1)} + \frac{\sigma_{\dot{h}}^{(1)}}{z_{\dot{h}}} \nabla \tilde{C}_{\dot{h}}^{(1)} \right) \tag{15d}$$

$$\tilde{C}_{\dot{h}}^{(1)} = 1 \tag{15e}$$

$$\tilde{C}_{e^-}^{(2)} = \left(\frac{p_{O_2}^{(2)}}{p_{O_2}^{(1)}} \right)^{1/4} \tag{15f}$$

Eq. (15d) was obtained by combining Eqs. (6), (7) and (10) written for respective charge species. The conductivity, $\sigma_i = z_i^2 F^2 u_i c_i$ at the electrolyte boundary can be expressed as a function of temperature and oxygen partial pressure [11], i.e.

$$\sigma_{V_{\ddot{O}}} = \sigma_{V_{\ddot{O}}}^{O} \exp\left(\frac{\Delta H_{V_{\ddot{O}}}}{kT} \right) \tag{16}$$

$$\sigma_{e^-} = \sigma_{e^-}^{O} p_{O_2}^{-1/4} \exp\left(\frac{E_{e^-}}{kT} \right) \tag{17}$$

$$\sigma_{\dot{h}} = \sigma_{\dot{h}}^{O} p_{O_2}^{1/4} \exp\left(\frac{E_{\dot{h}}}{kT} \right) \tag{18}$$

Table 1 shows typical electrical conductivities and activation energies used in this study.

The differential Eqs. (12)–(14) do not yield any analytical solution but can be solved by a numerical method. Once the distribution of species concentration is determined, the ionic current density and electronic current density (both contributions of free electrons and electron holes) flowing through the electrolyte can be obtained. Thus,

$$I_i = \sigma_{V_{\ddot{O}}} \nabla \phi^{(1)} \tag{19}$$

$$I_e = (\sigma_{e^-}^{(2)} \tilde{C}_{e^-} + \sigma_{\dot{h}}^{(1)} \tilde{C}_{\dot{h}}) \nabla \phi^{(1)} + \frac{R_u T}{F} \left(\frac{\sigma_{e^-}^{(2)}}{z_{e^-}} \nabla \tilde{C}_{e^-}^{(1)} + \frac{\sigma_{\dot{h}}^{(1)}}{z_{\dot{h}}} \nabla \tilde{C}_{\dot{h}}^{(1)} \right) \tag{20}$$

Under open-circuit conditions ionic current is equal to the electronic current.

3. Results and discussion

All simulation results refer to the operating conditions of SoFCs and CoGs. For SoFCs, the oxygen partial pressure is set to 0.21 atm at the cathode side and 10^{-18} atm (balanced by hydrogen and water vapour pressures) at the anode side. For CoG, two systems, $CO + CO_2$|electrolyte|pure O_2 and $N_2 + O_2$|electrolyte|pure O_2 are considered. The former is an indicative gas composition for Mars, and the latter for Earth. Two electrolytes, doped-ZrO_2 and doped-Bi_2O_3, are examined.

The distributions of the dimensionless concentration of free electrons and electron holes across the electrolyte are given in Fig. 2. On the high oxygen pressure side ($y/L = 0$), the conductivity is due mainly to the electron holes, while on the low oxygen pressure side ($y/L = 1$) it is due mainly to the free electrons. Since an equilibrium condition exists between free electrons in the conduction band and electron holes in the valence band (annihilation), the intersection of the concentration curves of free electrons and electron holes is expected at a certain point, δ, in the electrolyte. This critical point shifts from the high ($y/L = 0$) to the low oxygen partial pressure side ($y/L = 1$) whenever $p_{O_2}^{(1)}$ or $p_{O_2}^{(2)}$ increases. With a known distribution of electronic charge concentrations, the electronic currents due to the respective diffusion of free electrons

Table 1
Electrical conductivities and activation energies of selected electrolytes

Electrolyte	Temperature range (°C)	$\sigma_{V_{\ddot{O}}}^{O}$ (S cm^{-1})	$\Delta H_{V_{\ddot{O}}}$ (eV)	$\sigma_{e^-}^{O}$ (S cm^{-1})	E_{e^-} (eV)	$\sigma_{\dot{h}}^{O}$ (S cm^{-1})	$E_{\dot{h}}$ (eV)	Reference
ZrO_2 + 8 mol% Y_2O_3	700–1200	1.63×10^2	0.79	1.31×10^7	3.88	2.5	1.67	[12]
BiO_3+20 mol% M_2O_3[a]	500–700	8.68×10^4	1.08	2.59×10^5	2.24	580.4	1.12	[13]

[a] M_2O_3: Er_2O_3 or Y_2O_3.

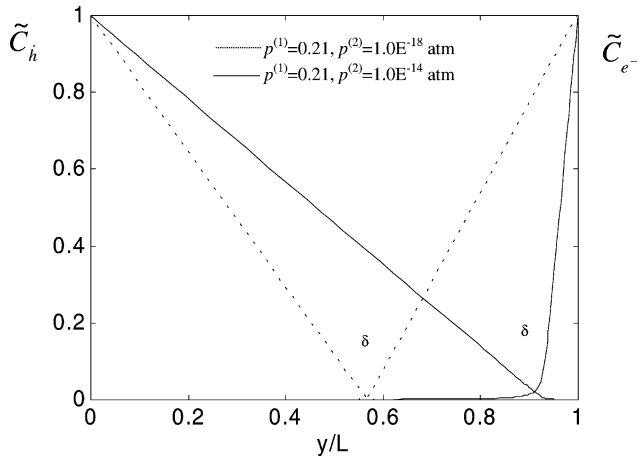

Fig. 2. Distributions of dimensionless concentration of free electrons and electron holes along the electrolyte thickness.

and electron holes can be calculated; the results are given in Fig. 3. Along the thickness of electrolyte from the high to the low oxygen partial pressure, the electrolyte changes from a p-type semiconductor to an n-type semiconductor. This phenomenon can be used to distinguish the contribution of free electrons and electron holes to the total electronic conductivity of the electrolyte by semi-permeability measurements [5].

As was discussed above, the electronic current due to the diffusion of free electrons and electron holes is compensated by the counter-flow oxygen ions. The rate of oxygen semi-permeation is determined by the electronic current that flows through the electrolyte and can be expressed as:

$$J_{O_2} = \frac{I_e}{4F} \tag{21}$$

where I_e can be determined from Eq. (20).

The effect of electrolyte thickness on the oxygen semi-permeability for doped-ZrO_2 and doped-Bi_2O_3 electrolytes is presented in Fig. 4. It was found that for both the doped-ZrO_2 and doped-Bi_2O_3, the oxygen semi-permeability is linearly proportional to the reciprocal of the electrolyte thickness. When $L \to \infty$, the oxygen semi-permeability trends to zero. Compared with the doped-ZrO_2 at 1000 °C, the oxygen semi-permeability of doped-Bi_2O_3 at 600 °C for a 0.2 mm thickness ($1/L = 5$) is about twice as high. It is also noted that the higher the operating temperature, the higher is the semi-permeability. As we will discuss later, the semi-permeability will cause different performance characteristics of the SoFC and CoG.

To study the impact of conductivity on oxygen semi-permeability, the electronic and ionic conductivities of the electrolyte are varied arbitrary. The effect of the conductivity on the oxygen semi-permeability using the values from Table 2 is given in Fig. 5.

Comparing curves A and B, though the ionic conductivity is increased by 10 times in curve B, the oxygen semi-permeability is only marginally higher. Comparing curves A and C, however, if both the free-electron and electron–hole conductivities are increased by two times in the latter, the corresponding oxygen semi-permeability also increased by as much. This phenomenon is particularly useful for the selection of electrolyte materials for use in gas-separation devices. For ionic domain materials, the effective way to increase the oxygen semi-permeability is to improve the electronic conductivity of the materials. Some researchers have successfully developed high oxygen permeation composites with mixed electronic and ionic conductors [14–16].

We arbitrarily assume that pure CO_2 at 1 atm is fed to the cathode side of a CoG simulating the Mars atmosphere. If

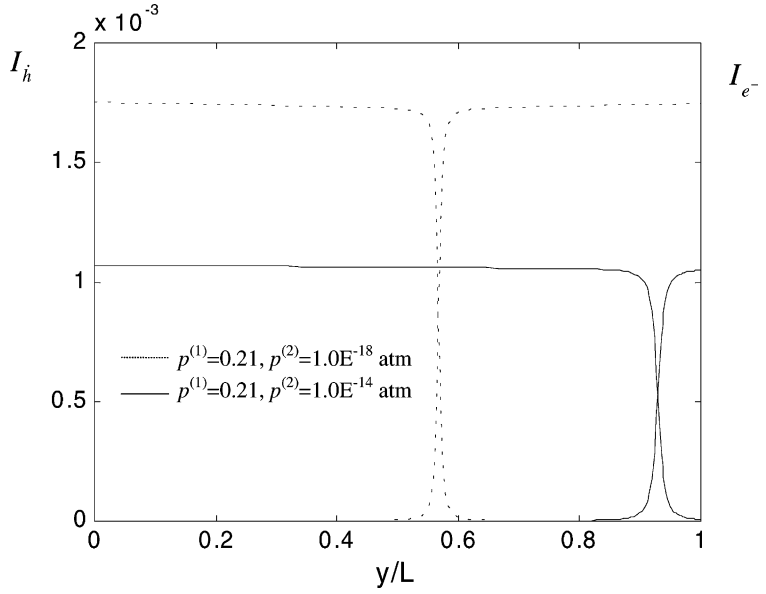

Fig. 3. Distributions of electronic currents along electrolyte thickness.

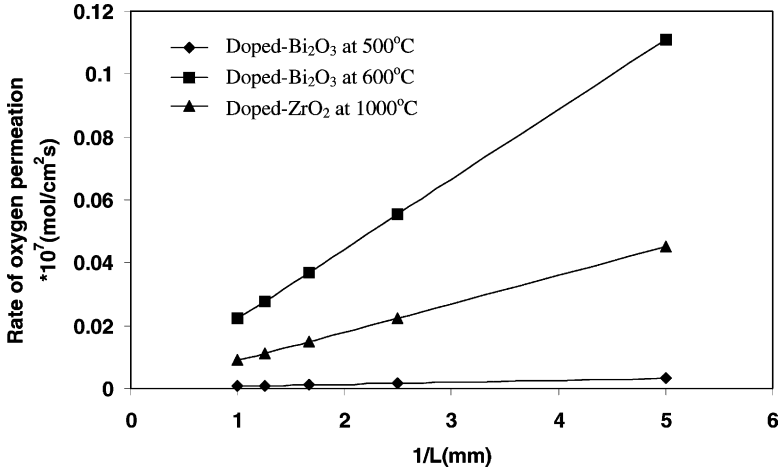

Fig. 4. Effect of electrolyte thickness on oxygen permeation at open-circuit.

Table 2
Electrical conductivities used for in Fig. 5

Curve	σ_{e^-} (S cm^{-1})	$\sigma_{\dot{h}}$ (S cm^{-1})	$\sigma_{v_{\ddot{o}}}$ (S cm^{-1})
A[a]	1.77×10^{-4}	1.82×10^{-4}	0.12
B	1.77×10^{-4}	1.82×10^{-4}	1.2
C	3.54×10^{-4}	3.64×10^{-4}	0.12

[a] The conductivities used in curve A are based on doped-ZrO_2 at 1000 °C and is considered as the baseline for comparison.

the concentration gradients of CO_2 and CO at the cathode surface are neglected, the pressure of CO on the cathode surface with a drawn current density of I and a CO_2 flow velocity of υ is given by

$$p_{CO} = \frac{n_{CO}R_uT}{V} = \frac{n_{CO}J_{CO}R_uT}{\upsilon} = \frac{IR_uT}{F\upsilon} \quad (22)$$

Thus, the oxygen partial pressure at the cathode side can be calculated for any temperature based on equilibrium thermodynamics [3], i.e.

$$p_{O_2} = \left[\frac{p_{CO_2}}{p_{CO}} \times 1.75 \times 10^4 \times \exp\left(-\frac{2.82 \times 10^5}{R_uT}\right)\right]^2 \quad (23)$$

At open circuit ($I = 0$) $p_{O_2} = 2p_{CO_2}$ and Eq. (23) can be rewritten as:

$$p_{O_2} = \left[\frac{p_{CO_2}}{2} \times 3.5 \times 10^4 \times \exp\left(-\frac{2.82 \times 10^5}{R_uT}\right)\right]^{2/3} \quad (24)$$

The effect of temperature on the oxygen semi-permeability for different electrolyte thicknesses at open-circuit is shown in Fig. 6a and b. In Fig. 6a, $p_{O_2}^{(1)}$ is calculated from Eq. (24) and $p_{O_2}^{(2)}$ is set to 1 atm. To simulate the CO + CO_2|electro-CoG system, while in Fig. 6b $p_{O_2}^{(1)}$ and $p_{O_2}^{(2)}$ are set to 0.21 and 1 atm, respectively, to simulate the $N_2 + O_2$|electrolyte|pure O_2 CoG system. Results show that the rate of oxygen permeation of doped-Bi_2O_3 electrolyte with a thickness of 0.2 mm increases monotonically with increasing temperature and reaches 1.523×10^{-8} and 0.202×10^{-8} mol

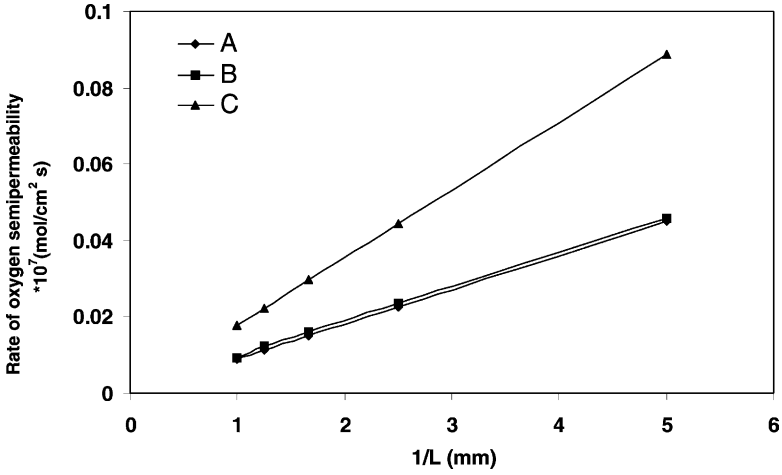

Fig. 5. Sensitivity of electrical conductivity on oxygen semi-permeability.

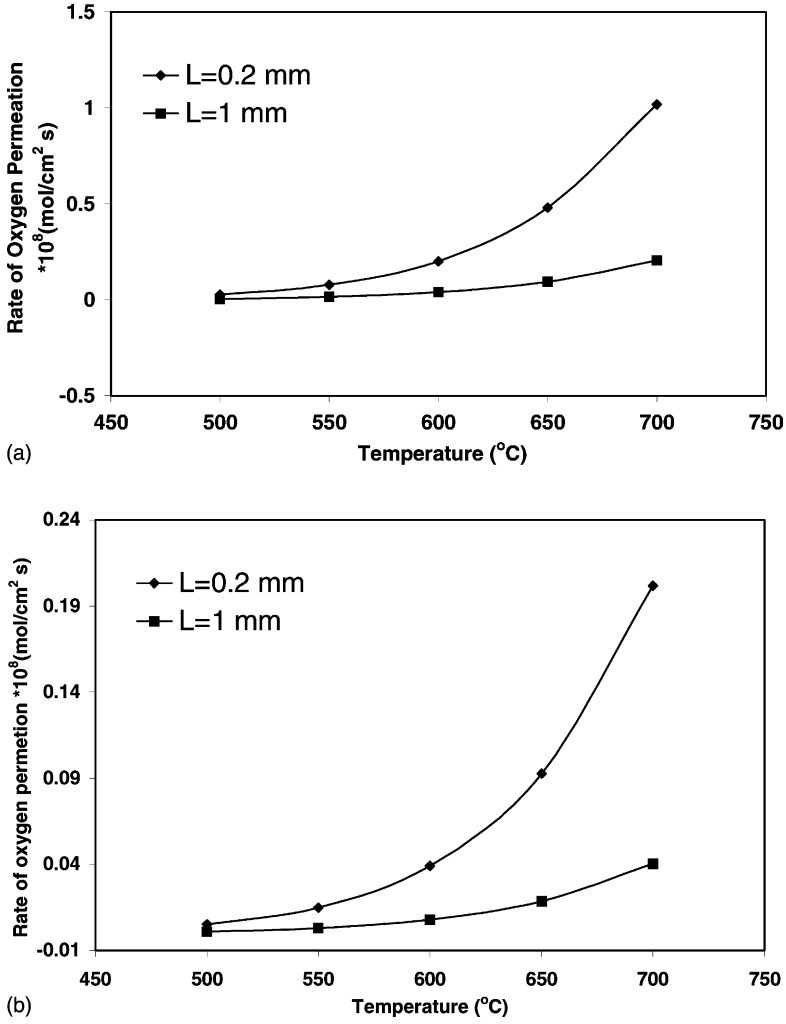

Fig. 6. (a) Effect of temperature on oxygen permeation at open-circuit for $CO + CO_2$|doped-Bi_2O_3|O_2 CoG system. (b) Effect of temperature on oxygen permeation at open-circuit for $N_2 + O_2$|doped-Bi_2O_3|O_2 CoG system.

$cm^2\ s^{-1}$, respectively, at 700 °C for the two systems. For all temperatures, more oxygen permeation can be expected for thinner electrolytes, which agrees with the results shown in Fig. 4.

The effect of current density on the rate of oxygen generation for the $CO + CO_2$|electrolyte|pure O_2 CoG system is given in Fig. 7. Due to the oxygen semi-permeability from the pure oxygen side to the $CO + CO_2$ side, which is in the opposite direction of the ionic flow due to current applied, the actual oxygen produced in doped-Bi_2O_3 at 700 °C is lower than the amount expected. Because of the low electronic conductivity in doped-ZrO_2 at 1000 °C, the actual oxygen produced is almost same as the theoretical value. In the case of the $N_2 + O_2$|electrolyte|pure O_2 CoG system, the migration of oxygen ions due to semi-permeation is in the same direction as the migration of oxygen ions due to current applied. Hence, the oxygen semi-permeability behaviour of the electrolyte is actually beneficial to the generation of the oxygen. Results in Fig. 8 show that the doped-Bi_2O_3 based CoG can actually produce more oxygen than the theoretical amount. Thus, selection of electrolyte materials for CoG application should consider the operating environment and the working principle of the CoG to maximise the oxygen yield.

When ion-conducting membrane is used in a SoFC, efficient operation of the fuel cell requires the ionic conductivity to be much higher than its electronic counterpart in the electrolyte. The equivalent circuit of a SoFC is given in Fig. 9 and includes consideration of electronic conduction in the electrolyte. The output power density of the fuel cell is given by

$$P_{out} = I_{out} \times E_{out} \tag{25}$$

The rate of total energy input to the SoFC is the summation of the electrical power output (P_{out}) and the Joule heating due to the Ohmic losses associated with ionic flow (P_i), electronic flow (P_e), anode polarisation (P_A) and cathode polarisation (P_C). Thus,

$$\begin{aligned} P_{total} &= P_i + P_e + P_A + P_C + P_{out} \\ &= I_{out}E_{out} + I_i^2R_i + I_e^2R_e + I_A^2R_A + I_C^2R_C \end{aligned} \tag{26}$$

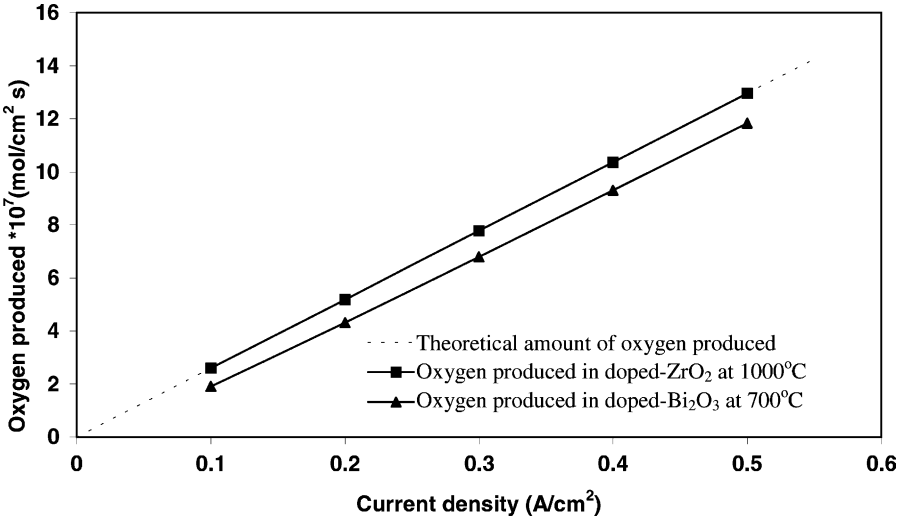

Fig. 7. Effect of current density on oxygen generation rate for different electrolyte materials used in $CO + CO_2$|doped-Bi_2O_3|O_2 CoG system.

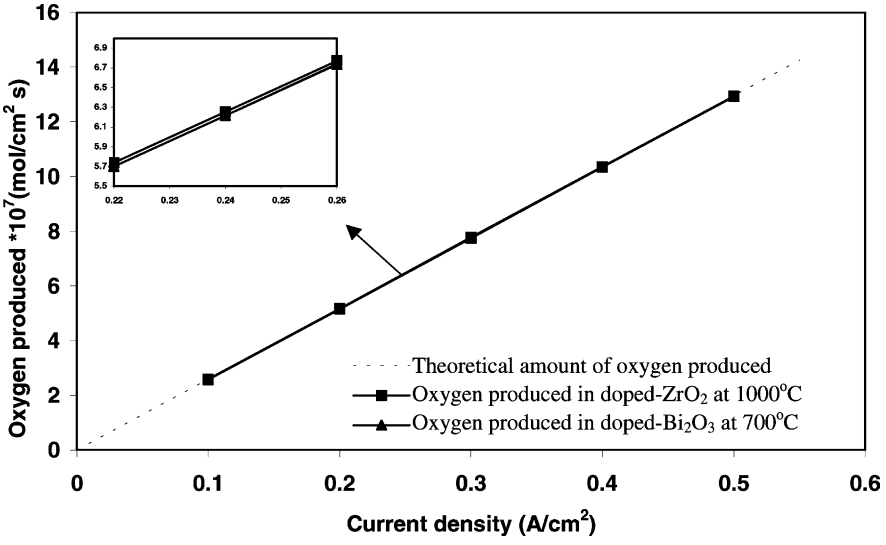

Fig. 8. Effect of current density on oxygen generation rate for different electrolyte materials used in $N_2 + CO_2$|doped-Bi_2O_3|O_2 CoG system.

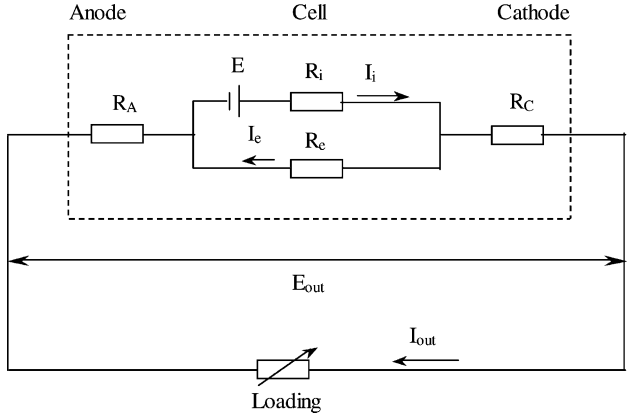

Fig. 9. Equivalent circuit of SoFC including electronic conduction of electrolyte.

The energy efficiency, ε, is defined the ratio of the electrical power output to the rate of total energy input to the fuel cell, i.e.

$$\varepsilon = \frac{P_{\text{out}}}{P_{\text{total}}} = \frac{I_{\text{out}}E_{\text{out}}}{I_{\text{out}}E_{\text{out}} + I_{\text{i}}^2R_{\text{i}} + I_{\text{e}}^2R_{\text{e}} + I_{\text{A}}^2R_{\text{A}} + I_{\text{C}}^2R_{\text{C}}} \tag{27}$$

The effect of the current density on energy efficiency and output power density is illustrated in Figs. 10 and 11, respectively, for doped-ZrO_2 at 800 °C. The thinner the electrolyte, the higher the output power density and energy efficiency will be at intermediate current density. In addition, the peak energy efficiency shifts towards lower current densities for a thicker electrolyte. As shown above (Fig. 4), the rate of oxygen semi-permeability (or the electronic current density) decreases with increase in electrolyte

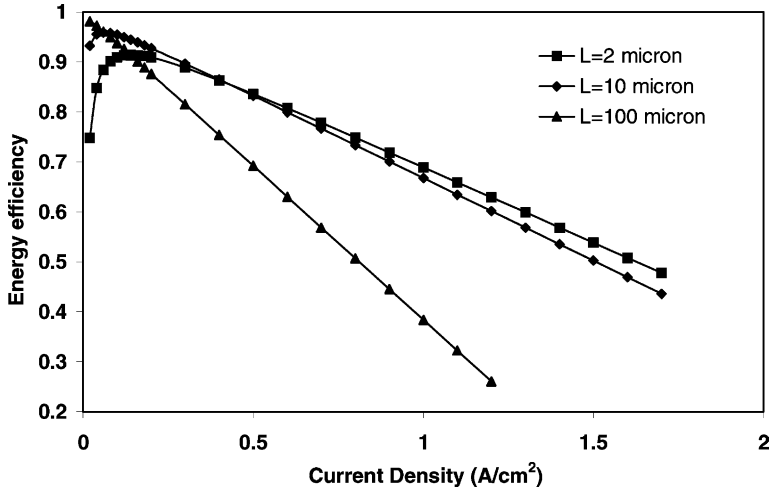

Fig. 10. Energy efficiency as a function of current density for different doped-ZrO_2 electrolyte thickness (operation at 800 °C).

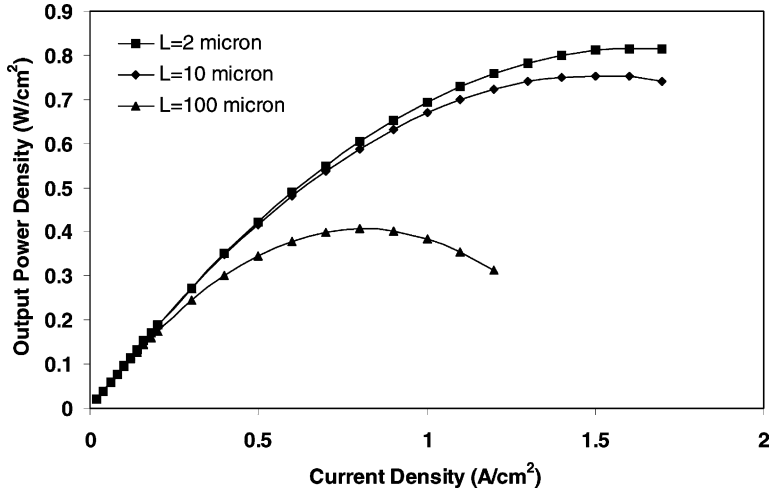

Fig. 11. Output power density as a function of current density for different doped-ZrO_2 electrolyte thickness (operation at 800 °C).

thickness. Thus, the effect of electrolyte thickness on energy efficiency depends on the combined losses due to the electrolyte resistance and the oxygen semi-permeability. For an electrolyte of ionic conductivity, such as doped-ZrO_2, the Ohmic loss dominates the energy efficiency of the fuel cell at intermediate current density.

4. Conclusions

An electrolyte model for ion-conducting membranes used in ceramic oxygen generators and solid oxide fuel cells has been developed. The model, which consists of a set of three second-order differential equations and six boundary conditions, establishes the relationships between the potential and the concentrations of free electrons and electron holes along the thickness of the electrolyte. It facilitates the study of various electrolyte materials as well as the effects of operating temperature, oxygen partial pressure and electrolyte thickness on the oxygen semi-permeability. The model is used to analyse the effect of oxygen semi-permeability on the performance of a CoG and SoFC. The contribution of free electrons and electron holes to the total electronic conductivity depends highly on the oxygen partial pressure at the gas|electrolyte interface. For ionic domain electrolyte, the oxygen semi-permeability is mainly influenced by the electronic conductivity of the electrolyte. An effective way to enhance the throughput of a differential oxygen generator is to use a material with high electronic conductivity for improved oxygen semi-permeability. In addition, high oxygen semi-permeability can be achieved with high operating temperature, high differential oxygen pressure, or a thinner electrolyte. For a $CO + CO_2$|electrolyte|pure O_2 CoG system, it is desirable to use an electrolyte with low oxygen semi-permeability because the oxygen semi-permeation is in counter direction to the ionic flow under applied current.

For a $N_2 + O_2$|electrolyte|pure O_2 CoG system, however, high oxygen semi-permeability is desirable as oxygen semi-permeation is in the same direction of the ionic flow under applied current. In a SoFC with doped-ZrO_2 at 800 °C, the thinner the electrolyte, the higher is the energy efficiency at intermediate current density because of the higher Ohmic loss of the electrolyte.

References

[1] A.V. Virkar, J. Electrochem. Soc. 138 (1991) 1481.
[2] F.M.B. Marques, L.M. Navarro, Solid State Ionics 90 (1996) 183.
[3] K.R. Sridhar, B.T. Vaniman, Solid State Ionics 93 (1997) 321.
[4] Y. Mishima, H. Mitsuyasu, M. Ohtaki, K. Eguchi, J. Electrochem. Soc. 145 (1998) 1004.
[5] M. Kleitz, E. Fernandez, J. Fouletier, P. Fabry, in: A.H. Heuer, L.W. Hobbs (Eds.), Science and Technology of Zirconia III, Vol. 3, American Ceramic Society, Columbus, OH, 1981, p. 349.
[6] R.T. Brook, in: A.H. Heuer, L.W. Hobbs (Eds.), Science and Technology of Zirconia III, Vol. 3, American Ceramic Society, Columbus, OH, 1981, p. 1.
[7] N.Q. Minh, T. Takahashi, Science and Technology of Ceramic Fuel Cells, Elsevier, Amsterdam, The Netherlands, 1995, pp. 69–101.
[8] H. Iwahara, T. Esaka, T. Mangahara, J. Appl. Electrochem. 18 (1998) 73.
[9] Y. Teraoka, T. Nobunaga, K. Okamoto, N. Miura, N. Yamazoe, Solid State Ionics 48 (1991) 207.
[10] H.W. Brinkma, H. Kruuidhof, A.T. Burggraaf, Solid State Ionics 68 (1994) 173.
[11] N.Q. Minh, T. Takahashi, Science and Technology of Ceramic Fuel Cells, Elsevier, Amsterdam, The Netherlands, 1995, pp. 50–55.
[12] J.H. Park, R.N. Blumenthal, J. Electrochem. Soc. 136 (1989) 2867.
[13] T. Takahashi, T. Esaka, H. Iwahara, J. Appl. Electrochem. 7 (1977) 303.
[14] H. Naito, H. Yugami, H. Arashi, Solid State Ionics 90 (1996) 173.
[15] C.S. Chen, H. Kruidhof, H.J.M. Bouwmeester, H. Verweij, A.J. Burggraaf, Solid State Ionics 99 (1997) 215.
[16] V.V. Kharton, A.V. Kovalevsky, A.P. Viskup, F.M. Figueiredo, A.A. Yaremchenko, E.N. Naumovich, F.M.B. Marques, Solid State Ionics 21 (2001) 1763.